RESEARCH ARTICLE

Parameter Selection Guidelines for Direct-on-Line Permanent Magnet Generators Contemplating Fault-Ride-Through Capability

PIETU KINNUNEN[1]**, PIA LINDH**[ID][1]**, (Senior Member, IEEE), DANIIL ZADOROZHNIUK**[1]**, JUHA PYRHÖNEN**[ID][1]**, (Senior Member, IEEE), AND ASKO PARVIAINEN**[2]

[1]Department of Electrical Engineering, Lappeenranta-Lahti University of Technology, 53850 Lappeenranta, Finland
[2]Danfoss Editron Oy, 53500 Lappeenranta, Finland

Corresponding author: Pia Lindh (pia.lindh@lut.fi)

ABSTRACT Direct-on-line (DOL) driven permanent-magnet generators (PMSGs) are often applied in small-scale hydropower plants (<10 MW). The Commission Regulation (EU) 2016/631 defines the boundary conditions to operate these generators in parallel with the grid. According to the regulation, fault-ride-through (FRT) capability is required in some cases. FRT scenario of PMSGs was studied by simulations and the importance of machine parameters was analyzed. Machine parameters under interest are damper winding resistance and leakage inductance, stator resistance and leakage inductance, saliency, source voltage, total inductance and system inertia. Authors proved that fault-ride-through can be achieved by utilizing smart machine parameters selection without using complicated control systems and auxiliary equipment. FRT simulations are performed for three PMSGs and their capabilities are explored. Results can be used as a guideline in DOL PMSG design for satisfying FRT requirements. The simulation system was also verified with measurements of a 600 kW PMSG data during a fault situation: an incident where the generator was connected to the grid in phase opposition.

INDEX TERMS Direct-on-line, electrical machine design, permanent magnet generator, fault ride through capability.

I. INTRODUCTION

Permanent magnet synchronous generators (PMSGs) offer an interesting alternative in small-scale hydropower as they achieve superior efficiency by eliminating the rotor excitation power. The benefit is most drastic in low-head hydropower plants, where low-speed machinery is required. These machines, however, bring some challenges as the reactive power of the generator cannot be controlled. If voltage or reactive power control is required, direct-on-line (DOL) PMSGs without a separate compensator device are out of question. This research is focused on Direct-on-line (DOL)

The associate editor coordinating the review of this manuscript and approving it for publication was Venkateshkumar M[ID].

grid connection system, which doesn't require multi-stage gearbox because a low-speed high-torque synchronous generator is used. The other types of generating grid-connected systems can be: Fixed-speed turbine system, which has a squirrel-cage induction generator (SCIG) directly connected to the grid and multistage gearbox and a doubly fed induction generator (DFIG) system, in where the stator winding is directly connected to the grid, but the rotor winding uses power electronic converter. [1]

New generators must operate in accordance with the Commission Regulation (EU) 2016/631 and corresponding local regulations [2]. These regulations set requirements depending on the significance of the power plant for the synchronous area in question. Power plants are rated in types

A, B, C, and D, which have different definitions in different regions depending on the nominal connection point voltage and power. Categories A or B are valid for small-scale hydropower and DOL PMSGs. However, in category B a voltage control system is required, so in principle a separate compensator would be needed. In categories C and D, conventional synchronous machines are likely to be techno-economically more practical. According to the FRT capability requirement of the regulation, generators in categories B and above should be capable of remaining connected and continuing stable operation after a secured fault. Transmission system operators (TSO) specify the relevant boundaries within the ranges shown in Fig. 1 and Table 1.

Fault-ride-through parameters presented in Fig. 1 are: U_{ret} is the retained voltage at the connection point during a fault, U_{clear} is the lower voltage limit at fault clearance, U_{rec1} and U_{rec2} are the lower voltage limits after the clearance, t_{clear} is the time instance for fault clearance and t_{rec1}, t_{rec2} and t_{rec3} are time instances for the voltage limits. In addition, it is possible that national grid codes prohibit momentary pole slipping during a FRT event [3]. The pole slip can presumably be defined in this context as a case where a generator exceeds the load angle δ value of 180 degrees. The load angle is defined as the angle between permanent magnet flux linkage ψ_{PM} and stator flux linkage ψ_s.
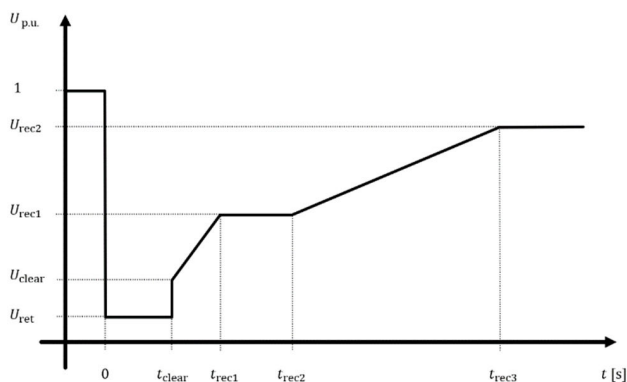
FIGURE 1. Fault-ride-through profile in a three-phase fault. Line-to-line voltage (per-unit) as a function of time (s) during a symmetrical fault. (modified from [1]).

TABLE 1. Fault-ride-through parameters (modified from [2]).

Voltage parameters [pu] for types B and C		Time parameters [s] for types B and C	
U_{ret}	0.05–0.3	t_{clear}	0.14–0.15 (or 0.14–0.25 if system protection and secure operation so require)
U_{clear}	0.7–0.9	t_{rec1}	t_{clear}
U_{rec1}	U_{clear}	t_{rec2}	t_{rec1}–0.7
U_{rec2}	0.85–0.9 and $\geq U_{clear}$	t_{rec3}	t_{rec2}–1.5

FRT capability studies have mainly focused on systems incorporating a power electronic converter with a control scheme, extra protective components or conventional synchronous machines [4], [5], [6], [7], [8], [9], [10], [11], [12]. The control methods lately studied are e.g. a FRT scheme for wind energy system is recently introduced in [13]. This approach combines an event-triggered sliding mode control (ETSMC) with a super-capacitor and a high-frequency magnetic linked dual active bridge converter. Nonlinear Adaptive Backstepping Controller [14] and a simple but working method, which includes resetting the distributed generation and network protection relays to create conditions to meet the FRT requirements [15]. Latest protective components studies were held on hybrid superconducting fault current limiter with bias magnetic field [16] and Optimal Shunt-Resonance Fault Current Limiter [17].

In previous studies, generator parameters affecting FRT are mentioned e.g. in [18] by introducing a stator damping resistor or [19] a dynamic braking resistor. In [20] protection by crowbar in stator design is utilized. The effect of generator parameters in case of DOL systems are widely studied in [21] and the effect of damper windings in DOL generator designing in [22]. Comparison and analysis of the fault characteristics of squirrel-cage-inductor-generator wind farms and DOL permanent magnet generator wind farms under different fault conditions is presented in [23], which gives some directions for generator parameter selections.

There are only few studies on criteria definition for FRT. One comprehensive research is found in [24], which gives a literature pertaining to FRT and low voltage ride-through (LVRT). This paper highlights network characteristics, technologies and international LVRT practices and presents VRT criteria in different countries. A control strategy for LVRT and HVRT capability enhancement for grid connected solar system is proposed in [25] and experimental verified to be effective.

Authors' earlier study [26] gives designing guidelines for DOL PMG (used in a hydro-power system) parameters: inductances, level of back electromotive voltage, starting current, short circuit fault tolerance and customer requirements for network codes. However in [26] authors does not discuss FRT issues. Some guidelines for designing PM machines in DOL system are provided in [27] and [28].

The main interest of this article is therefore focused on selecting the most suitable generator parameters to minimize FRT problems. In this study FRT capability of DOL PMSGs is investigated and the aim is to find design recommendations to achieve the required FRT performance with DOL PMSG. In our study, fault event was extensively simulated while the machine parameters were varied. This paper is based on work done as a part of [29]. In [29] the requirements that potentially cause constraints of the design for permanent magnet machine DOL system are identified, and necessary simulation scenarios are sorted out, considering also FRT. Some findings from [29] are utilized to develop the guidelines.

The research methodology is first described in Section 2. It also explains the structure and boundaries of the simulation tool built in the MATLAB/Simulink®environment. Then the

simulations are verified with the aid of real measurement data and finally the main results are presented in Section 4.

II. METHODOLOGY

The simulation comprising generator and grid model is built in the MATLAB/Simulink®environment utilizing lumped parameter circuit-models. Full details and pictures of it can be found in [30]. The traditional dq-axis generator model is utilised for calculating parameters, Fig. 2. Both axes have a damper circuit, which has a core influence on parameter selection for successful fault-ride-through.
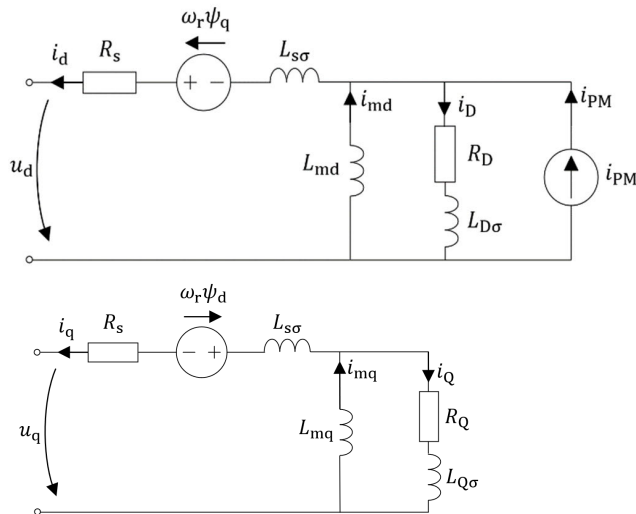
FIGURE 2. D- and q-axis equivalent circuits (modified from [28]). $i_{d,q}$ are the stator currents, $u_{d,q}$ are the stator terminal voltages, R_s is the stator resistance, $L_{s\sigma}$ is the stator leakage, $L_{md,q}$ are the magnetizing inductances, $R_{D,Q}$ are the damper winding resistances, $L_{D,Q\sigma}$ are the damper winding leakage inductances, $i_{D,Q}$ are the damper winding currents, $i_{md} = i_{PM} + i_D + i_d$ is the d-axis magnetizing current, and $i_{mq} = i_Q + i_q$ is the q-axis magnetizing current.

The equations of the simulation tool are written in the rotor reference frame, in where the axes rotate along with the rotor, and therefore the electric and magnetic quantities are constants at steady state. Fig. 3 illustrates a corresponding vector diagram. Phase quantities of a three-phase system can be converted to the rotor reference frame by equations originally presented by R.H. Park

$$\begin{bmatrix} X_d \\ X_q \\ X_0 \end{bmatrix} = \frac{2}{3} \begin{bmatrix} \cos(\theta) & \cos\left(\theta - \frac{2\pi}{3}\right) & \cos\left(\theta + \frac{2\pi}{3}\right) \\ -\sin(\theta) & -\sin\left(\theta + \frac{2\pi}{3}\right) & -\sin\left(\theta - \frac{2\pi}{3}\right) \\ \frac{1}{2} & \frac{1}{2} & \frac{1}{2} \end{bmatrix} \begin{bmatrix} X_{L1} \\ X_{L2} \\ X_{L3} \end{bmatrix}, \quad (1)$$

where X represents a quantity that is converted and θ is the position angle, and phases are marked with L1, L2 and L3.

The reference frame speed can be solved with (1). The position angle θ in rotor frame is

$$\theta_r = \int \omega r dt = \int p\Omega r dt, \quad (2)$$

where ωr is the electrical rotor angular velocity, p the number of pole pairs and ωr the mechanical rotor angular velocity. Initial parameters of the model are set as follows: with an open stator, $u_{s,d}$ is set to zero and u_q to e_{PM}. The flux linkages have the initial values $\psi_d = \psi_D = -\psi_{PM}$ and $\psi_q = \psi_Q = 0$. Only PM-produced flux linkage is present, inducing voltage on the q-axis of the rotating generator. The resistances and permanent magnet flux linkage values are adjusted based on the temperature. The absolute value of the electromagnetic torque is calculated as a cross product of the stator flux linkage and the stator current. In electrical part simplifications are related to the fact, that the model doesn't consider iron losses nor saturation, because they would require far too much computation time.

Electric network is modelled as an infinite bus in the simulation tool. The grid voltage is given as a reference to the generator model. The simulations are made keeping the regulation in mind, so that the voltage profile of a fault dictates and considers the grid properties.
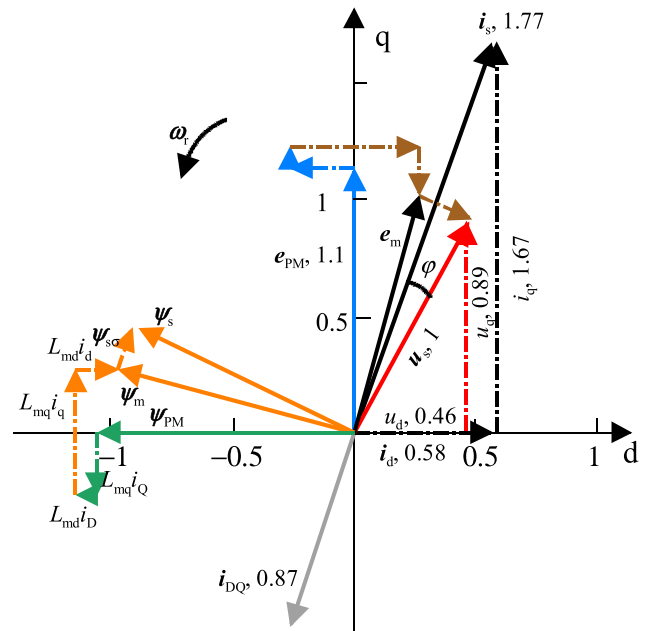
FIGURE 3. Transient-state vector diagram of a PMSG. ω_r is the angular velocity of the rotor, φ is the power-factor angle, ψ_{PM} is the permanent magnet flux linkage, ψ_s is the stator flux linkage, ψ_m is the air gap flux linkage, $L_{md}i_D$, $L_{mq}i_Q$ are the damper winding reactions, L_{md} i_d-, L_{mq} i_q are the armature reactions, $L_{s\sigma}i_s$, is the stator leakage flux linkage, and e_{PM}, e_s, e_m, e_{mD}, e_{mQ}, e_{md}, e_{mq}, $e_{s\sigma}$ are the corresponding electromagnetic forces.

Rotating inertia is modelled as a first-order differential equation of motion, with a stiff shaft as

$$\Omega = \int \frac{T_{turb} - T_e - D_{tot}\Omega}{J_{tot}} dt, \quad (3)$$

where Ω is the mechanical angular velocity, T_{turb} is the torque produced by the prime mover, T_e is the electromagnetic torque, J_{tot} is the total system moment of inertia and D_{tot} is the total system friction coefficient. The prime mover torque is given as an input value to the mechanical model. Thereby this model doesn't take into account mechanical oscillations. A two-mass model could be used if mechanical resonances are of interest [30].

To verify the model, a case where 600 kW PMSG was connected to an electric network in phase opposition was simulated and the result was compared with the measured waveform presented in Fig. 4. Furthermore, comparisons between known theory and the behaviour of the model are given in [30].
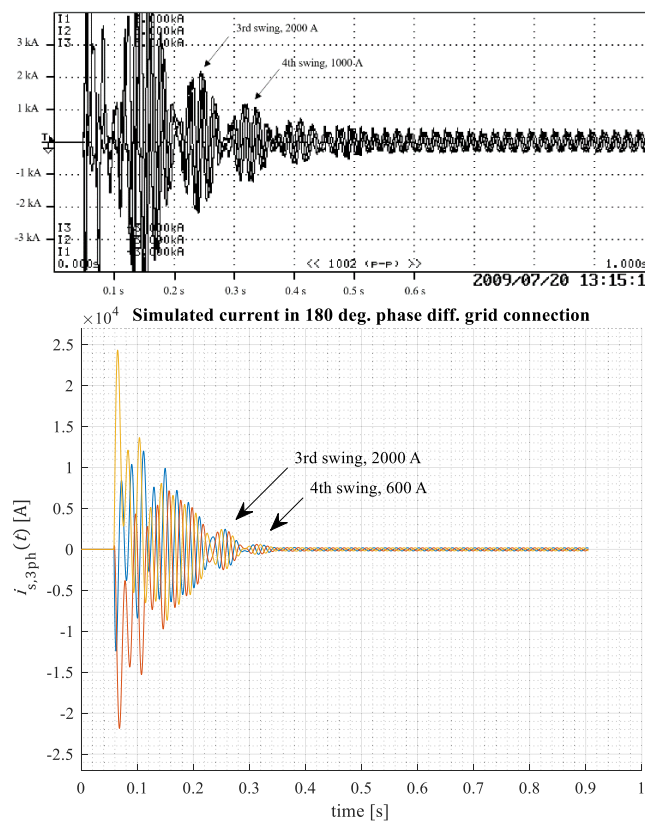
FIGURE 4. Recorded (top) and simulated PMSG grid connection in phase opposition. $L_{s\sigma}$ = 95.5 μH (0.1156 pu), L_{md} = 249.5 μH (0.3021 pu), L_{mq} = 264.51 μH (0.3202 pu), $L_{D\sigma}$ = $L_{Q\sigma}$ = 0, J_{tot} = 251.2 kgm^2, D_{tot} = 3 Nms/rad, R_s = 0.0036 Ω (0.0140 pu), R_D = 9.60 mΩ (0.0370 pu), R_Q = 8.97 mΩ (0.0346 pu).

In the context of this study, it would be beneficial to have experimental data from a FRT event, but the required measurement preparations would be enormous as on-site testing would be needed. Power plant owners are most likely to be reluctant to risk damaging their devices if not necessary. Furthermore, the relevant grid operator may not even allow such tests to be performed. To study a real transient existing measurement data from phase-opposite grid connection fault was used. This extreme transient event seems to be

even more severe than a three-phase short circuit fault since momentary voltage across the stator resistance is at maximum when connection is made, and that makes current and torque to be significantly higher. It is considered to be rare to obtain measurement data of faults like the one shown in Fig. 4 because such measurements are normally not made on purpose, especially with an expensive generator. The data was obtained, unfortunately, only in a form of image, from the accident where incorrectly configured synchronization device was used.

The specifications sheet parameters of the machine are listed in Table 2. Unluckily, the information available is not as detailed as the model, and therefore, some additional assumptions were needed. In general, manufacturers tend to limit the details they provide to protect their core competences [31].

TABLE 2. Reported parameters of the PMSG connected with a phase difference of 180 degrees.

Quantity	Value
Rated active power P_n	600 kW
Rated frequency f_n	50 Hz
Rated rotational speed n	300 rpm
PM-induced voltage (line-to-line) E_{PM}	430 V
Rated current I_n	890 A
DC resistance R_s (20 °C)	3.642 mΩ (0.0140 pu)
d-axis synchronous inductance L_d	345 μH (0.4177 pu)
q-axis synchronous inductance L_q	360 μH (0.4359 pu)
Sustained short-circuit current i_{ssc}	3077 A
Subtransient short-circuit current i_s''	8235 A
Subtransient reactance X_d''	0.030 Ω (0.1156 pu)
Damper winding reactance referred to stator	0.081 Ω (0.3122 pu)
Damper winding resistance referred to stator	8.97 mΩ (0.0346 pu)
Generator moment of inertia J_g	157 kgm^2

The parameters for the model were obtained based on Table 2 as follows: The damper winding inductances were set equal to the magnetizing inductances assuming, thus, zero leakage ($L_{D\sigma} = L_{Q\sigma} = 0$). The stator leakage inductance value was set to correspond to the subtransient inductance $L_{s\sigma} = L_d'' = (0.030\Omega/(2 \cdot \pi \cdot 50\mathrm{Hz}) = 95.5\ \mu$H. The magnetizing inductances were calculated as $L_{md} = L_{sd} - L_{s\sigma} = 345\ \mu$H $- 95.5\ \mu$H $= 249.5\ \mu$H, $L_{mq} = L_{sq} - L_{s\sigma}\ 360\ \mu$H $- 95.5\ \mu$H $= 264.5\ \mu$H. The manufacturer indicated that the d-axis damper winding resistance is slightly higher than the q-axis resistance. Based on that information, the initial value $R_{D,Q} = 8.97$ mΩ was varied in the simulation to see whether the similarity between the simulation and the measurement increases. Finally, the following values were adopted: $R_Q = 8.97$ mΩ, $R_D = 9.60$ mΩ. The total moment of inertia of the system was set to 160% of the inertia of the generator, resulting in 1.6×157 kgm^2, and the total friction was set to 3 Nms/rad. A line-to-line voltage of 405 V at 50 Hz frequency was used.

Synchronization starting in phase opposition produces high currents and stresses. However, the PMSG still managed to synchronize and settle to no-load as it can be seen in Fig. 4. The recorded and simulated currents have similar patterns with periodically varying amplitudes. The phase-opposition

connection of the generator was not performed on purpose, and therefore, the currents significantly exceed the capacity of the measurement system. Therefore, a direct amplitude comparison is not possible. The simulation result attenuates roughly at the same pace as the recorded currents. The waveforms are slightly different because the parameters have uncertainty due to unknown tolerances and previously mentioned assumptions. Also, constant parameters were used which generally cannot produce fully accurate results. In addition, grid properties can affect the waveform. It could be possible to achieve even better resemblance between the simulated and measured waveforms by carrying out full parameter identification tests for the machine, but that is not possible since the machine is in use.

It is important to understand that in reality the generator parameters vary depending on the operating status of the machine. For more accurate simulation, transient FEA should be used. However, it would be too time consuming for the repeated FRT simulations. The accuracy of the lumped parameter model can be considered acceptable when used to identify general system behavior.

Three different machines representing a baseline are introduced in Table 3. The introduced machines are of type A or B depending on the installation location. For type A power plants, the FRT capability is not required, but meeting the requirement would still be beneficial. The stator leakage inductance corresponding to X_d'' has the same value as in Section 3 except for the 1300-125 machine, where $L_{\mathrm{s}\sigma} = L_\mathrm{d}/3$ was used. The accuracy of the initial parameters is irrelevant because they serve only as a comparative baseline for investigating the effect of parameter variation.

TABLE 3. The reference machines.

Quantity	340-250	520-600	1300-125
Rated active power P_n, kW	340	520	1300
Rated apparent power S_n, kVA	355	542	1310
Rated input torque T, kNm	13.5	8.6	106
Generator moment of inertia J_g, kgm^2	169	25	2900
Turbine moment of inertia J_t, kgm^2	101	32	2560
Rated frequency f_n, Hz	50	60	50
Rated rotational speed n, rpm	250	600	125
Number of pole pairs p	12	6	24
Rated speed PM-induced line-to-line voltage E_PM, V	430	510	730
Grid voltage, V	400	480	690
Rated current I_n, A	510	650	1100
Temperature class	F	F	F
Stator resistance R_s, mΩ	6.7	5.5	5
Stator resistance R_s, pu	0.015	0.013	0.014
Direct-axis and Quadrature-axis synchronous inductance L_q, mH	0.8	0.86	0.55
Direct-axis L_d and Quadrature-axis synchronous inductance L_q, pu	0.555	0.760	0.477
Subtransient d-axis reactance X_d'', mΩ	58.9	111	170
Subtransient d-axis reactance X_d'', pu	0.13	0.26	0.47
Subtransient d-axis time constant τ_d'', s	0.06	0.02	0.11
Damper winding direct-axis R_D and quadrature axis resistance R_Q, mΩ	22.6	25.6	39.8
Damper winding direct-axis R_D and quadrature axis resistance R_Q, pu	0.05	0.06	0.11

The FRT simulations were performed with following initial operating conditions:

- Friction is set to 3 Nms/rad.
- FRT profile of a three-phase fault with [U_ret, U_clear, U_rec1, U_rec2] = [0.05, 0.7, 0.7, 0.85], [t_clear, t_rec1, t_rec2, t_rec3] = [0.25, 0.25, 0.7, 1.5] is supplied as a voltage reference. This is the largest voltage sag shown in the regulation.
- The pre-fault conditions are defined by the relevant TSO, but in this case, generators rated points are used (Table 3).
- Turbine torque remains constant during FRT. This assumption is reasonable for purposes of this study, but for a more detailed analysis, the power plant related turbine speed-torque performance characteristics should be implemented into the model. For example, if the turbine torque decreases at super synchronous speeds, the acceleration during a fault will not be as severe.
- Stator and rotor temperatures are set to 100 °C and 50 °C before the fault initiation and are not updated during the fault.
- The variable-step solver in Simulink® 2019b is used with a maximum step size of 0.0003 s and a relative tolerance of 1e-6. Decreasing the maximum step size further did not have a notable effect on the simulation outcome.
- Criteria for synchronism: The following must be true for 0.04 s after the t_rec3 time instance: $|slip|$ < 0.02, $|I_\mathrm{DQ,pu}|$ < 0.01, $|\mathrm{d}\delta/\mathrm{d}t|$ < 2. If synchronism is not detected within 4 s after the t_rec3 or Ω > $3\Omega_\mathrm{n}$ or Ω < 0 at any time, the test has failed.
- FRT is simulated as a pass/fail test repeatedly while the PMSG parameters are varied in loops. Also the synchronization time after the fault and the maximum fault duration or fault clearance time seem to be suitable performance metrics for some cases.
- Because the process is computationally heavy, the number of nested loops for different parameters must be limited. Truly exhaustive survey where all the relations between different parameters are inspected is not feasible. The results must also be reasonably easy to analyze and realistically exportable to the design of a machine.
- Temporary pole slip is allowed in the tests because it seems very difficult otherwise to pass the test as stated in the regulation with a DOL PMSG. One reason is a high stator current, which produces a large stator leakage flux linkage, increasing the load angle and therefore electromagnetic torque in addition to the rotor acceleration. Based on the simulations, synchronism can still be restored because of the damper winding if such operation can be tolerated.

Examples of successful FRT for 340-250 machine under the above-stated terms are shown in Fig. 5 and Fig. 6.

With the initial parameters, none of the machines passed the test. The 340-250 machine was, however, very close to success, and a small damper winding resistance reduction

(from $R_{D,Q} = 22.6$ mΩ (0.05 pu) to $R_{D,Q} = 22.3$ mΩ (0.0492 pu)) was enough to pass the FRT test. In Fig. 5 and Fig. 6, a pole slip takes place, but synchronism is still eventually restored right in four seconds after fault initiation when the excess rotational energy in the rotor is fed to the grid. This is possible mainly because of the operation of damper winding. However, quite large oscillations are present. Examples of failed FRT are presented in Fig. 7 and Fig. 8. The failure was produced by gradually reducing the rotor inertia.
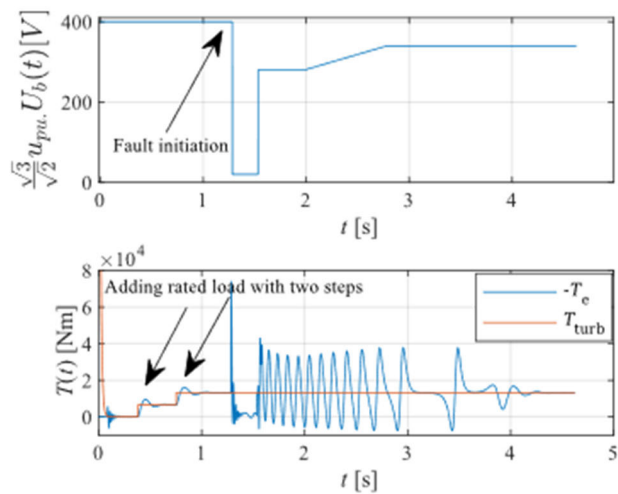
FIGURE 5. Voltage and torque diagrams in case of successful FRT with 340-250 machine. A temporary pole slip is allowed.
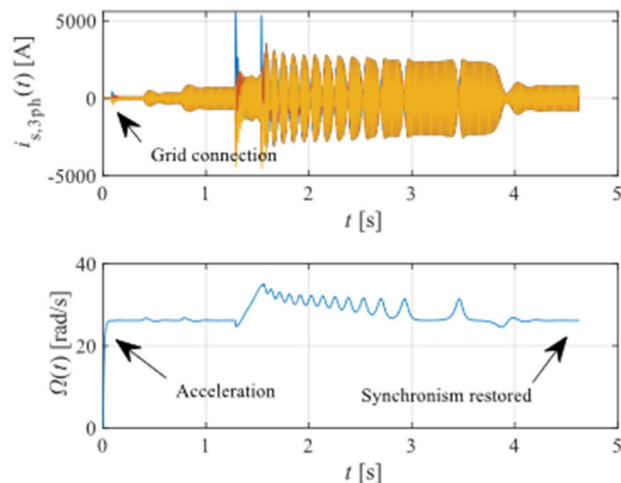
FIGURE 6. Current and speed diagrams in case of successful FRT with 340-250 machine. A temporary pole slip is allowed.

III. SIMULATION RESULTS
This section presents the influence of different parameter values on successful FRT. The results are based on the idea that synchronism can be restored by the operation of the damper winding even if a temporary pole slip occurs. The results are presented as graphs for the most interesting cases of 340-250
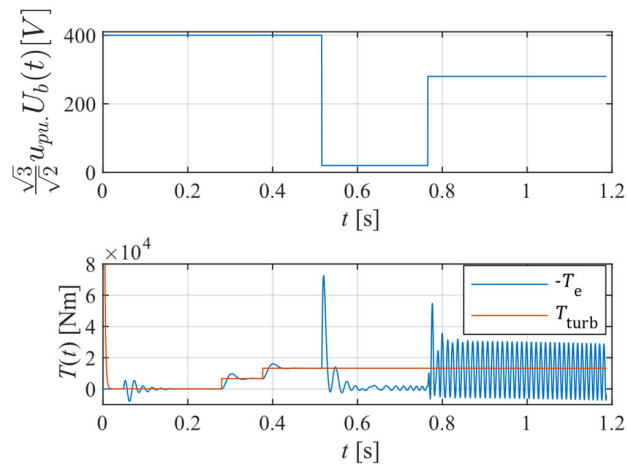
FIGURE 7. Voltage and torque diagrams in case failed FRT with 340-250 machine.
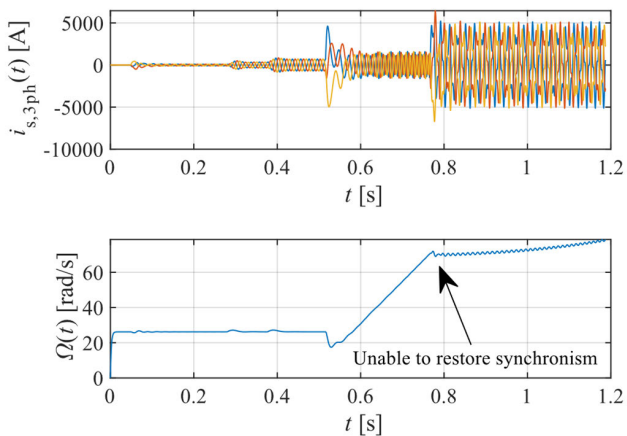
FIGURE 8. Current and speed diagrams in case failed FRT with 340-250 machine.

machine. All simulation are done with the most difficulties fault profiles. The base values that are used to calculate the per unit values correspond to the initial parameters list.

A. DAMPER WINDING RESISTANCES
The effects of varying damper winding resistance are shown in Fig. 9. It may contain unrealistic datapoints because R_D and R_Q depend on each other. The 520-600 machine did not pass the test with any damper winding resistance values, and in the case of 1300-125 the green area was similar in shape but much smaller (0.07 – 0.08 pu).

The damper resistances have a great impact on the capability of restoring synchronism. According to the results, the resistances should be close to 0.04 pu in this case.

B. DAMPER WINDING LEAKAGE INDUCTANCES
Damper leakage inductance values from 0 to $0.5 \times L_{s\sigma}$ were tested. All machines failed in FRT with the initial parameters, and the increased damper leakage made the performance
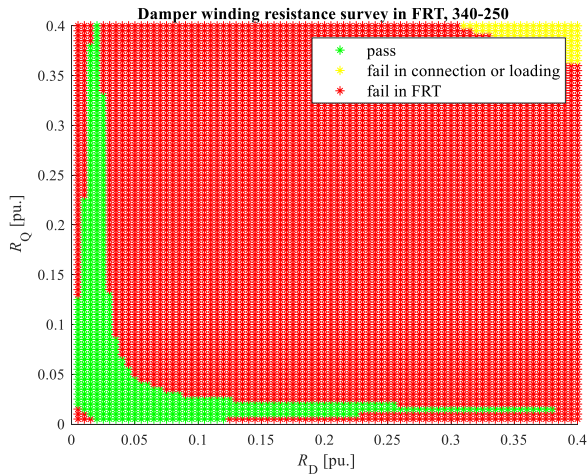
FIGURE 9. Study of damper winding resistance. The other parameter were kept at their initial values.

FIGURE 10. Study of damper winding resistance. $L_{D,Q\sigma} = 0.03$ pu.

even worse. Thus, damper winding leakage does not appear to be beneficial at all and should be minimized in machine design. This may be a somewhat difficult task since damper bars are normally placed in semi-closed slots. To minimize the leakage, open slots or even some sort of rotor surface positioning should be preferred. This may cause mechanical problems.

Damper winding resistance analysis of 340-250 machine was repeated with $L_{D,Q\sigma} = 0.03$ pu, Fig. 10. The test further indicates that the damper leakage is harmful to the FRT capability as the suitable resistance variation area is reduced compared with the $L_{D,Q\sigma} = 0$ pu results. The suitable resistance value area shrinks at the edges. This may be considered a positive finding because designing damper winding with a certain leakage is not an easy task. If damper resistances are correctly chosen, the leakage values do not seem to have a too large impact as long as they remain small.

C. SALIENCY

L_d/L_q values were tested with a fixed $L_{s\sigma}$ and a fixed maximum steady-state torque. The inductance ratio has a high significance for the machine design, and reluctance torque can help in FRT and enable lower PM material use. However, saliency can negatively affect the torque and back electromotive force quality as the armature reaction produces non-sinusoidal flux density in the air gap [27]. The effect of varying the inductance ratio is depicted in Fig. 11. The machines 520-600 and 1300-125 failed with all the inductance ratios tested. In these cases, a decreased inductance ratio does not bring major positive effects on FRT. For the 340-250 machine, the inverse saliency seemed to improve the FRT performance.

D. STATOR RESISTANCE

Stator resistance was varied between 0 and 0.08 pu. The $520 - 600$ machine failed with all stator resistance values, but the 340-250 and 1300-125 machines passed the test when
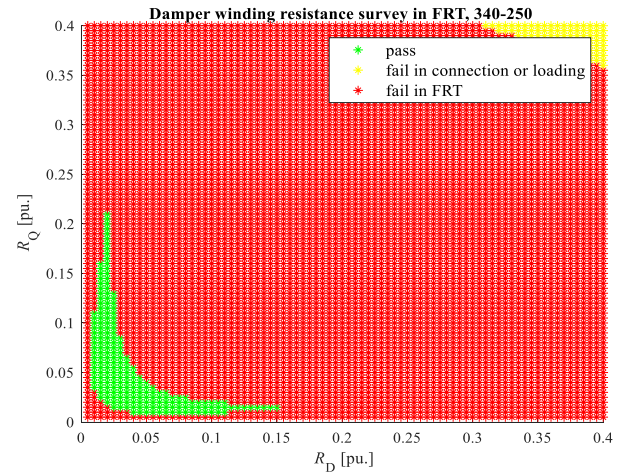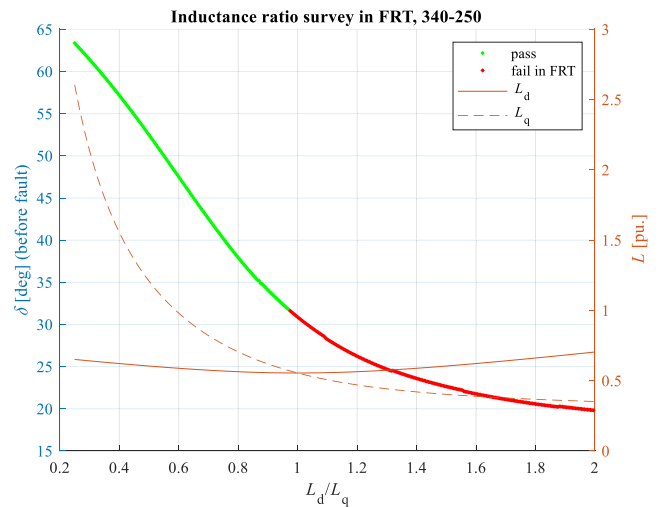
FIGURE 11. Study of the inductance ratio. Inductances are chosen to produce fixed maximum steady-state torque. The load angle before the fault is shown as reference data.

choosing a suitable R_s. However, no clear trend was found. The stator resistance strongly affects the machine efficiency and must thus be minimized. An acceptable FRT performance can be achieved by tuning machine parameters other than stator resistance.

E. SOURCE VOLTAGE

The PM flux linkage plays a key role in the machine performance. It affects E_{PM}, PQ operating point, peak torque, and short-circuit current. E_{PM} was varied in the range of $0.8 - 1.5$ pu. The inductances and the maximum steady-state torque were fixed by increasing the total inductances. The stator leakage and the L_d/L_q ratio were fixed.

Only the 340-250 machine was able to pass the FRT test when E_{PM} values were higher than 1.09 pu. With this approach, the load angle before a fault decreased considerably, which seems to be beneficial. There is, however, not much freedom to increase E_{PM} because it should be close to

the grid voltage. Further, the benefit of a smaller load angle before a fault is not very significant, if pole slipping occurs in any case and the restoration of synchronism relies mostly on the damper winding.

F. STATOR LEAKAGE INDUCTANCE

The share of stator leakage inductance in the range of $0.1 - 0.8$ of the total d-axis inductance was tested keeping the stator inductance value fixed. To obtain extra information, the maximum stator current and electromagnetic torque in a sudden short-circuit were chosen as reference data; they are strongly dependent on the stator leakage and consistent regardless of whether the FRT test is passed or not.

Fig. 12 demonstrates that a small stator leakage is beneficial for FRT; all machines were able to pass with a small stator leakage. This is challenging because high-pole-pair machines regularly have a high proportion of stator leakage inductance.
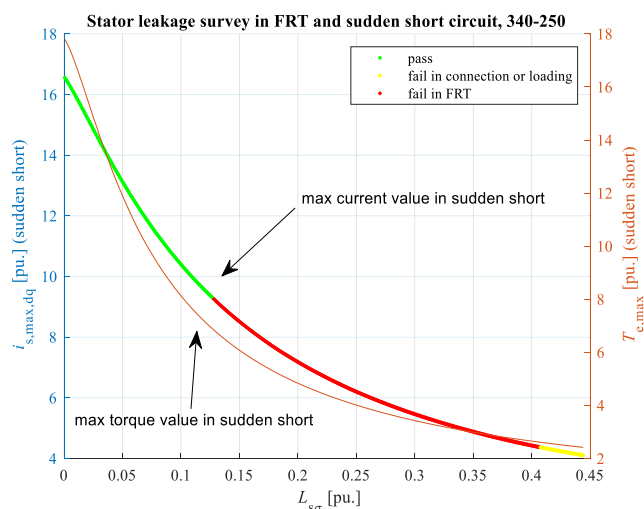
FIGURE 12. Study of stator leakage inductance.

G. TOTAL INDUCTANCE

The initial L_d/L_q and $L_{s\sigma}/L_d$ were fixed and the total inductance was varied in the range of $0.2 - 8$ pu. The purpose was to see whether it would be beneficial to oversize the steady-state maximum torque. There was no clear change from the baseline on the FRT capability with the 520-600 or 1300-125 machines. Decreasing the total inductances allowed the 340-250 machine to pass, but it was close to pass already with its original parameters, and therefore, oversizing the maximum steady-state torque does not seem the right solution.

H. REITERATING THE DAMPER WINDING RESISTANCE TEST AND COMBINING THE FINDINGS

The investigation of damper winding resistance was repeated for all the machines by suitably employing the above findings. The back emfs and stator resistances were kept at their initial values. L_d/L_q was set to 0.95 keeping the initial

steady-state maximum torque. Stator leakage inductance was set to $0.2 \times L_d$ and $L_{D,Q\sigma} = 0.1 \times L_{s\sigma}$. Results are shown in Fig. 13, which illustrates a surface plot of synchronization times in FRT and the maximum transient electromagnetic torque in FRT with different damper winding resistances. The time was measured from the beginning of the fault to the time instant at which the synchronism criteria were fulfilled.
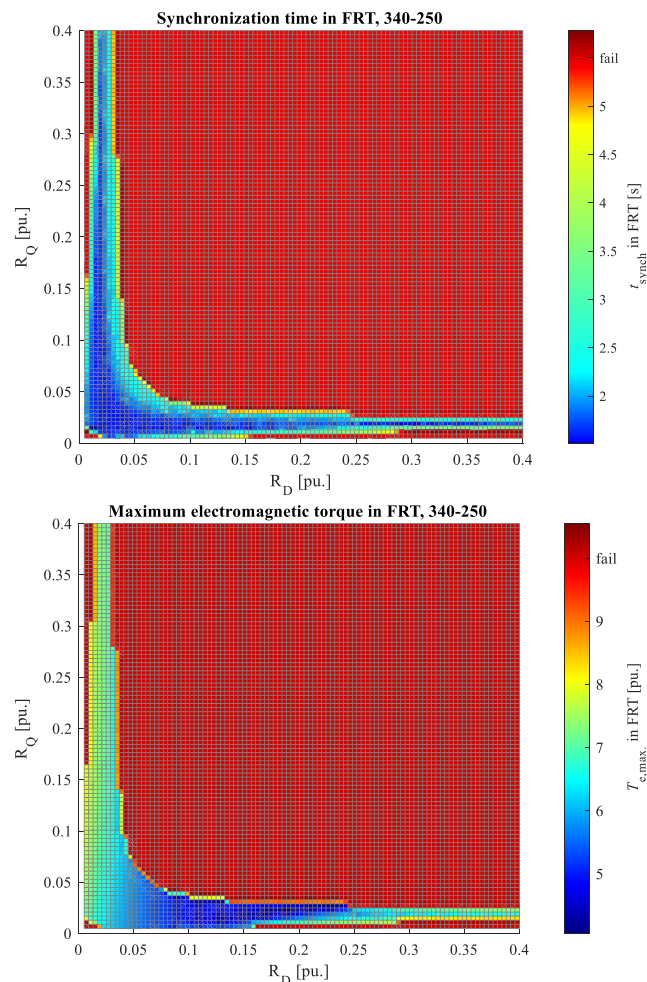
FIGURE 13. Studies of damper winding resistance with the modified parameters using the synchronization time in FRT as a performance metric and the maximum transient torque as reference data.

The use of the modified parameters enables a larger variance for damper winding resistances. If mechanical stresses are of concern, the transient torque can be decreased by increasing the damper d-axis resistance and using a relatively small q-axis resistance. Now also the $520 - 600$ machine narrowly passed the test. The damper winding resistance test was also carried out with different system inertia values. It was found that increased system inertia seems to shift and slightly reshape the suitable resistance area. Low inertia seems to favour higher resistance values.

The maximum acceptable fault duration using different $R_{D,Q}$ values with the $340 - 250$ machine was evaluated next. A fault profile time parameter scaling factor k_{fault} with

$k_{fault} = 1$ corresponding to the initial profile was introduced and the maximum fault duration for successful FRT was searched by trial and error, Fig. 14. This is somewhat different from how the concept of critical clearing time is commonly studied, because now it is considered that synchronism can be restored by relying on the damper winding even in the event of a pole slip.

As a performance metric, k_{fault} should get as high values as possible. However, higher values than $k_{fault} = 1$ are not needed. Even $k_{fault} = 0.6$ corresponding to $t_{clear} = 0.15$ s may be acceptable in some cases.
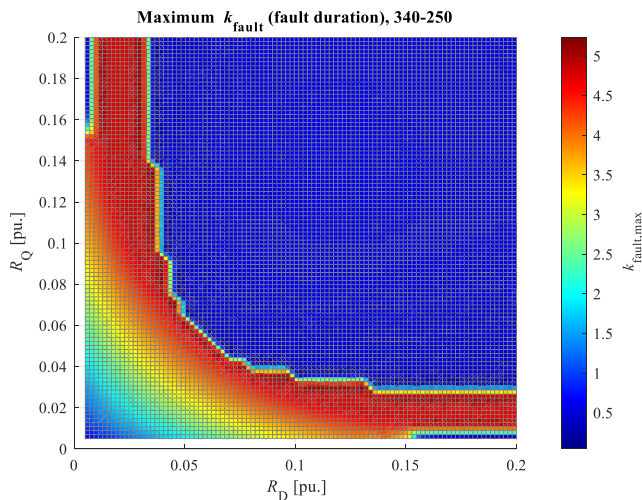
FIGURE 14. Damper winding resistance study using the fault time parameter k$_{fault}$ scaling factor as a performance metric. The higher the value is, the better the machine performs.

I. SYSTEM INERTIA

Inertia significance is evaluated by increasing the system inertia in the simulations. The damper resistances for the machines were chosen as: $340 - 250$: $R_{D,Q} = 0.029$ pu, $520 - 600$: $R_{D,Q} = 0.033$ pu, and $1300 - 125$: $R_{D,Q} = 0.028$ pu. Fig. 15 illustrates the results for the $340 - 250$ machine. The result for the two other machines were similar.

Some discontinuities can be seen in the synchronization time; they result from the definition of the synchronism conditions. Adding inertia reduces the speed fluctuation. However, if a pole slip occurs in any case, as in these tests, it can also cause the oscillations to attenuate poorly. Machine parameters must then correctly match the system inertia to restore synchronism.

J. TIME DOMAIN GRAPHS WITH THE MODIFIED PARAMETERS

Fig. 16 illustrates some time domain graphs of the FRT simulation with the $340 - 250$ machine to show the result of tuning the parameters based on the tests. Oscillation behaviour is significantly improved in comparison with Fig. 5 and Fig. 6. If such oscillations can be tolerated, the protection scheme should be designed accordingly [32].
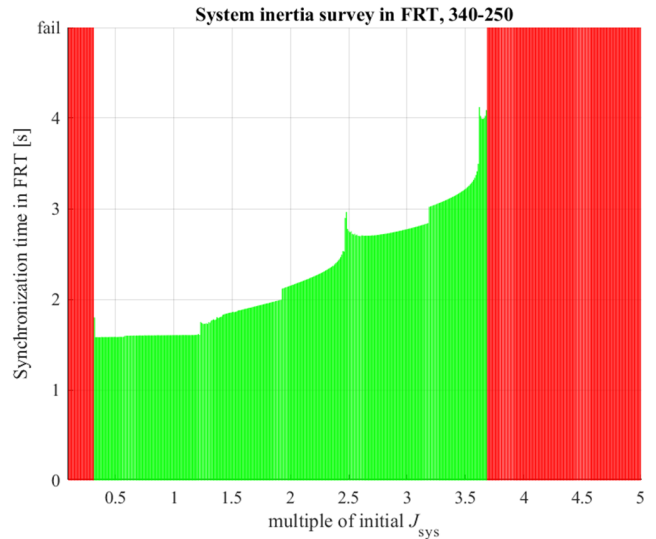
FIGURE 15. Damper Inertia study. The system inertia varies between 0 and 5 times the original value.
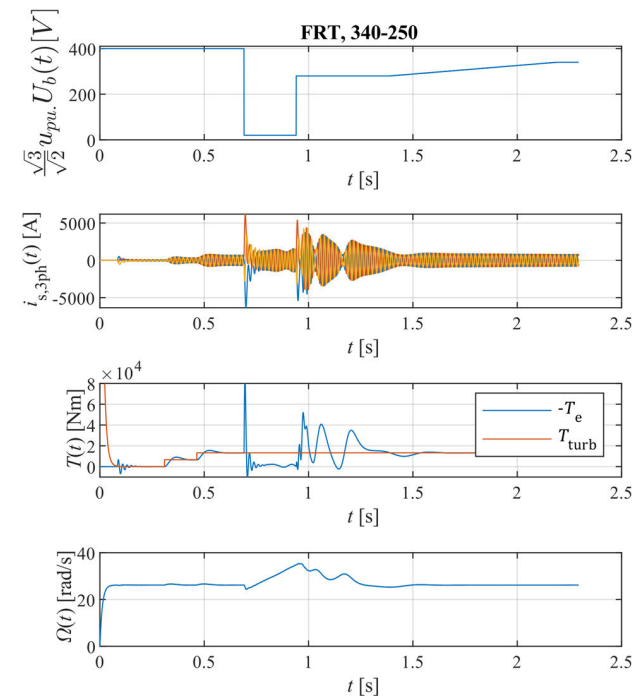
FIGURE 16. FRT simulation of the 340-250 machine with adjusted parameters. $L_{s\sigma} = 160.17$ μH (0.111 pu), $L_{md} = 640.69$ μH (0.445 pu), $L_{mq} = 682.84$ μH (0.474 pu), $L_{D\sigma} = L_{Q\sigma} = 16.02$ μH (0.0111 pu), $R_D = R_Q = 0.0131$ Ω (0.0290 pu).

IV. CONCLUSION

According to the simulation results it seems difficult to pass the FRT requirement of the Commission Regulation (EU) 2016/631 with a DOL PMSG without a temporary pole slip. However, a suitably designed damper winding may still be able to bring the machine back to synchronism in such a case.

If the temporary pole slip and the resulting strong oscillations can be tolerated, this kind of an approach to avoid disconnections might be a viable solution, at least for relatively small machines whose operation does not significantly affect other machines on the network.

When improving the FRT capability of a DOL PMSG, assuming that a temporary pole slip can be accepted, a designer should minimize the stator and damper winding leakage inductances and carefully choose the damper winding resistances. Inverse saliency can also be helpful in the task. The permanent-magnet-induced voltage can be selected mainly based on the rated operating point. Minimizing the synchronous inductance does not appear to be very beneficial. Damper winding leakage, instead, should be minimized, but it is less important if the damper resistance values are in the center of the region of suitable values of the (R_D, R_Q) map. Different damper winding resistances on the d- and q-axes can be used to limit the maximum transient torque if required. With a low system inertia, somewhat higher damper resistances seem to be required. In the case where a pole slip occurs, the system inertia must correctly match the electromagnetic design, and increasing the inertia is not necessarily beneficial.

Further work will be directed onto improving simulation model by analyzing other real fault simulations. A two-mass model could improve this model to analyze mechanical oscillations and more complicated grid presentation may be utilized in future work.

REFERENCES

[1] M. Nasiri, J. Milimonfared, and S. H. Fathi, "A review of low-voltage ride-through enhancement methods for permanent magnet synchronous generator based wind turbines," *Renew. Sustain. Energy Rev.*, vol. 47, pp. 399–415, Jul. 2015.

[2] *Establishing a Network Code on Requirements for Grid Connection of Generators*, document Commission Regulation (EU) 2016/631, The European Commission, Official Journal of the European Union, Brussels, Belgium, Apr. 2016.

[3] *Grid Code Specifications for Power Generating Facilities VJV2018*, Fingrid, Helsinki, Finland, Nov. 16, 2018.

[4] S. Gupta and A. Shukla, "Experimental study of fault impact on grid connected DFIG driven wind Turbine," in *Proc. IEEE Global Conf. Comput., Power Commun. Technol. (GlobConPT)*, Sep. 2022, pp. 1–6.

[5] E. Bekiroglu and M. D. Yazar, "Improving fault ride through capability of DFIG with fuzzy logic controlled crowbar protection," in *Proc. 11th Int. Conf. Renew. Energy Res. Appl. (ICRERA)*, Sep. 2022, pp. 374–378.

[6] M. Pouresmaeil, A. Sepehr, B. A. Khan, J. Adabi, and E. Pouresmaeil, "Model predictive-based control technique for fault ride-through capability of VSG-based grid-forming converter," in *Proc. 24th Eur. Conf. Power Electron. Appl. (EPE ECCE Eur.)*, Sep. 2022, pp. 1–7.

[7] P. Piya, M. Ebrahimi, M. Karimi-Ghartemani, and S. Khajehoddin, "Fault ride-through capability of voltage-controlled inverters," *IEEE Trans. Ind. Electron.*, vol. 65, no. 10, pp. 7933–7943, Jul. 2018, doi: 10.1109/TIE.2018.2803765.

[8] M. Eskandari and A. Savkin, "On the impact of fault ride-through on transient stability of autonomous microgrids: Nonlinear analysis and solution," *IEEE Trans. Smart Grid*, vol. 12, no. 2, pp. 999–1010, Mar. 2021, doi: 10.1109/TSG.2020.3030015.

[9] D. Ye, Z. Hao, T. Wang, and J. Hu, "State-space modeling of dual active bridge converters during fault ride-through operation," in *Proc. IEEE 13th Int. Symp. Power Electron. Distrib. Gener. Syst. (PEDG)*, Jun. 2022, pp. 1–5.

[10] A. A. Salem, A. A. Eldesouky, A. A. Farahat, and A. A. Abdelsalam, "New analysis framework of Lyapunov-based stability for hybrid wind farm equipped with FRT: A case study of Egyptian grid code," *IEEE Access*, vol. 9, pp. 80320–80339, 2021.

[11] S. Wang and L. Shang, "Fault ride through strategy of virtual-synchronous-controlled DFIG-based wind turbines under symmetrical grid faults," *IEEE Trans. Energy Convers.*, vol. 35, no. 3, pp. 1360–1371, Sep. 2020, doi: 10.1109/TEC.2020.2979885.

[12] P. Huang, M. El Moursi, and S. Hasen, "Novel fault ride-through scheme and control strategy for doubly fed induction generator-based wind turbine," *IEEE Trans. Energy Conv.*, vol. 30, no. 2, pp. 635–645, Jun. 2015, doi: 10.1109/TEC.2014.2367113.

[13] M. N. Musarrat, A. Fekih, M. A. Rahman, M. R. Islam, and K. M. Muttaqi, "A fault ride through scheme to improve the transient stability of wind energy systems," in *Proc. IEEE IAS Global Conf. Emerg. Technol. (GlobConET)*, May 2022, pp. 486–491.

[14] T. K. Roy, M. A. Mahmud, S. N. Islam, and A. M. T. Oo, "Nonlinear adaptive backstepping controller design for permanent magnet synchronous generator (PMSG)-based wind farms to enhance fault ride through capabilities," in *IEEE Power Energy Soc. Gen. Meeting (PESGM)*, Aug. 2019, pp. 1–5.

[15] V. C. Nikolaidis, N. Papanikolaou, A. S. Safigianni, A. G. Paspatis, and G. C. Konstantopoulos, "Influence of fault-ride-through requirements for distributed generators on the protection coordination of an actual distribution system with reclosers," in *Proc. IEEE Manchester PowerTech*, Jun. 2017, pp. 1–6.

[16] M. R. Islam, D. D. Abir, M. R. Islam, J. Hasan, M. N. Huda, K. M. Muttaqi, and D. Sutanto, "Enhancement of FRT capability of DFIG based wind farm by a hybrid superconducting fault current limiter with bias magnetic field," in *Proc. IEEE Int. Conf. Power Electron., Smart Grid Renew. Energy (PESGRE)*, Jan. 2020, pp. 1–6.

[17] A. M. A. Ibrahim, I. Hamdan, S. F. Al-Gahtani, H. S. Hussein, L. S. Nasrat, and M. A. Ismeil, "Optimal shunt-resonance fault current limiter for transient stability enhancement of a grid-connected hybrid PV/Wind power system," *IEEE Access*, vol. 9, pp. 126117–126134, 2021.

[18] A. A. Meri, Y. Amara, and C. Nichita, "Impact of fault ride-through on wind turbines systems design," in *Proc. 7th Int. Conf. Renew. Energy Res. Appl. (ICRERA)*, Oct. 2018, pp. 567–575.

[19] K. E. Okedu, S. M. Muyeen, R. Takakhashi, and J. Tamura, "Wind farms fault ride through using DFIG with new protection scheme," *IEEE Trans. Sustain. Energy*, vol. 3, no. 2, pp. 242–254, Apr. 2012.

[20] S.-W. Xu, Y. Dong, Y. Zhang, Y.-B. Wang, and S.-B. Yuan, "Protective strategy of crowbar circuit when network voltage drop sharply," in *Proc. 4th Int. Conf. Inf. Technol. Manage. Innov.*, China, Oct. 2015, pp. 377–383.

[21] J. Kinnunen, "Direct-on-line axial flux permanent magnet synchronous generator static and dynamic performance," Ph.D. dissertation, Acta Universitatis Lappeenrantaensis, Lappeenranta Univ. Technol., Lappeenranta, Finland, 2007.

[22] K. Kamiev, J. Nerg, and J. Pyrhonen, "Design of damper windings for direct-on-line permanent magnet synchronous generators," in *Proc. IEEE EUROCON*, May 2009, pp. 783–790.

[23] N. Liu, H. Gao, B. Xu, and Y. Wu, "Comparative analysis of wind field fault characteristics of squirrel-cage wind farms and direct-drive wind farms," in *Proc. 7th Asia Conf. Power Electr. Eng. (ACPEE)*, Apr. 2022, pp. 1533–1538.

[24] W. A. Qureshi and N. C. Nair, "Systematic development of low voltage ride-through (LVRT) envelope for grids," in *Proc. TENCON IEEE Region 10 Conf.*, Nov. 2010, pp. 574–579.

[25] C. Nithya and J. P. Roselyn, "Multimode inverter control strategy for LVRT and HVRT capability enhancement in grid connected solar PV system," *IEEE Access*, vol. 10, pp. 54899–54911, 2022.

[26] T. Lindh, P. Salminen, J. Pyrhonen, M. Niemela, J. Kinnunen, and J. Haataja, "Permanent magnet generator designing guidelines," in *Proc. Int. Conf. Power Eng., Energy Electr. Drives*, Apr. 2007, pp. 185–189.

[27] J. Pyrhönen, T. Jokinen, and V. Hrabovcovà, *Design of Rotating Electrical Machines*. Hoboken, NJ, USA: Wiley, 2014.

[28] K. Sindhya, A. Manninen, K. Miettinen, and J. Pippuri, "Design of a permanent magnet synchronous generator using interactive multiobjective optimization," *IEEE Trans. Ind. Electron.*, vol. 64, no. 12, pp. 9776–9783, Dec. 2017, doi: 10.1109/TIE.2017.2708038.

[29] P. Kinnunen, "Impact of grid code on design of a directly grid-connected permanent magnet generator," M.S. thesis, Dept. Elect. Eng., Lappeenranta-Lahti Univ. Technol., Lappeenranta, Finland, 2021.

[30] J. Kinnunen, "Direct-on-line axial flux permanent magnet synchronous generator static and dynamic performance," D.Sc. dissertation, Dept. Elect. Eng., Lappeenranta-Lahti Univ. Technol., Lappeenranta, Finland, 2007.

[31] I. Ristolainen, J. Simolin, N. Vägar, and M. Östman, "Considerations for fault ride through simulation and testing," POWERGEN Eur., Amsterdam, The Netherlands, Jun. 2015.

[32] R. Razzaghi, M. Davarpanah, and M. Sanaye-Pasand, "A novel protective scheme to protect small-scale synchronous generators against transient instability," *IEEE Trans. Ind. Electron.*, vol. 60, no. 4, pp. 1659–1667, Apr. 2013, doi: 10.1109/TIE.2012.2186773.

PIETU KINNUNEN received the Master of Science (M.Sc.) degree in electrical engineering from the Lappeenranta University of Technology (LUT), Finland, in 2021. He is currently working with the Department of Electrical Engineering, Lappeenranta-Lahti University of Technology.

PIA LINDH (Senior Member, IEEE) was born in Helsinki, in 1969. She received the M.Sc. degree in energy technology and the D.Sc. degree in electrical engineering (technology) from the Lappeenranta University of Technology (LUT), Lappeenranta, Finland, in 1998 and 2004, respectively. She is currently working as an Associate Professor at the Department of Electrical Engineering, LUT Energy, Lappeenranta, where she is engaged in teaching and research of electric motors and electric drives.

DANIIL ZADOROZHNIUK received the M.Sc. degree in electrical engineering from the Lappeenranta University of Technology, Finland, in 2022. He is currently a Junior Researcher with LUT University. His research interests include design and modeling of electrical machines and electrohydraulic devises.

JUHA PYRHÖNEN (Senior Member, IEEE) was born in Kuusankoski, Finland, in 1957. He received the Doctor of Science (D.Sc.) degree in electrical engineering from the Lappeenranta University of Technology (LUT), Finland, in 1991. He became a Professor in electrical machines and drives at LUT, in 1997. He is engaged in research and development of electric motors and power-electronic-controlled drives. He has wide experience in the research and development of special electric drives for distributed power production, traction drives, and high-speed applications. Permanent magnet materials and applying them in machines have an important role in his research. Currently, he is also researching new carbon-based materials for electrical machines.

ASKO PARVIAINEN received the M.Sc. and D.Sc. (Tech.) degrees in electrical engineering from the Lappeenranta University of Technology, Finland, in 2000 and 2005, respectively. He is currently a Senior Technology Manager at Danfoss Editron, Finland, specialized to a manufacturing of special purpose electric machines. His research interests include design and modeling of electrical machines, especially permanent magnet machines.

● ● ●